J Appl Electrochem (2008) 38:483–490
DOI 10.1007/s10800-007-9462-6

ORIGINAL PAPER

Supported Pt and Pt–Ru catalysts prepared by potentiostatic electrodeposition for methanol electrooxidation

J. M. Sieben · M. M. E. Duarte · C. E. Mayer

Received: 31 August 2007 / Revised: 8 November 2007 / Accepted: 24 November 2007 / Published online: 14 December 2007

Abstract Methanol electrooxidation was investigated on Pt–Ru electrocatalysts supported on glassy carbon. The catalysts were prepared by electrodeposition from solutions containing chloroplatinic acid and ruthenium chloride. Bulk composition analysis of the Pt–Ru catalyst was performed using an X-ray detector for energy dispersive spectroscopy analysis (EDX). Three different compositions were analyzed in the range 0–20 at.% Ru content. Tafel plots for the oxidation of methanol in solutions containing 0.1–2 M CH_3OH, and in the temperature range 23–50 °C showed a reasonably well-defined linear region. The slope of the Tafel plots was found to depend on the ruthenium composition. The lower slope was determined for the Pt catalyst, varying between 100 and 120 mV dec^{-1}. The values calculated for the alloys were higher, ranging from 120 to 140 mV dec^{-1}. The reaction order for methanol varies from 0.5 to 0.8, increasing with the ruthenium content. The activation energy calculated from Arrhenius plots was found to change with the catalyst composition, showing a lower value around 30 kJ mol^{-1} for the alloys, and a higher value, of 58.8 kJ mol^{-1}, for platinum. The effect of ruthenium content is explained by the bifunctional reaction mechanism.

Keywords Methanol · Platinum · Ruthenium · Electrodeposition · Catalyst

J. M. Sieben · M. M. E. Duarte (✉) · C. E. Mayer
Instituto de Ingeniería Electroquímica y Corrosión (INIEC), Universidad Nacional del Sur, Av. Alem 1253, 8000 Bahía Blanca, Argentina
e-mail: mduarte@criba.edu.ar

M. M. E. Duarte · C. E. Mayer
Comisión de Investigaciones Científicas de la Pcia de Buenos Aires, Buenos Aires, Argentina

1 Introduction

A direct methanol fuel cell (DMFC) based on a polymer electrolyte membrane is an attractive alternative for portable applications. However, several problems still hinder their practical uses. Developing more active catalysts for methanol oxidation, lowering the loading of noble metals catalysts and improving their effectiveness are keys to the success of this technology. To achieve this goal, it is necessary to increase the effective surface area of the catalysts, that is, to increase the surface contact between the catalyst, the electronic conductor (carbon), the electrolyte (a polymer cationic exchange membrane) and the reactant (methanol). The electrochemical reaction occurs in this active part of the electrodes and thus the performance depends significantly on the kinetics of interfacial phenomena [1, 2]. Usually, electrodes for proton exchange membrane fuel cells (PEMFC) are constituted of carbon powder, which acts as a catalyst support, and a solid polymer electrolyte such as Nafion® [3, 4]. In this case, to increase the performance of the electrodes one needs to increase the amount of catalyst, either increasing the thickness of the active layer or the catalyst loading in the catalytic powder. The use of thicker active layer leads to a decrease in the diffusion rate of the reactant towards the catalytic sites, whereas higher catalyst loading generally results in bigger catalyst particle size, thus decreasing their efficiency. Moreover, the utilization of catalysts in a Nafion® bonded anode is not high because the catalysts are not always in good contact with the electrolyte phase inasmuch as small pores may not be accessible to the ionomer [5].

One way to avoid these problems is to prepare electrodes by electrodeposition of metals at carbon electrodes. Electrodeposition in an aqueous solution offers an effective way to deposit platinum and other noble metal catalysts

selectively at desired locations in the electrode with both ionic and electronic access [6]. Electrodeposition with pulse current [1, 5, 7], direct current [8], constant potential or consecutive potential steps [9–18] and cyclic voltammetry [19, 20] have been used to deposit platinum and Pt–Ru bimetallic catalysts onto carbon substrates.

It is generally recognized that Pt–Ru alloys are the most active catalysts for methanol oxidation [21–23]. Optimum Ru content depends on temperature, potential range, and type of catalyst [24]. An increase in the optimum Ru content with temperature from 10 at.% Ru at 25 °C to 30 at.% Ru at 60 °C was determined for Pt–Ru alloys [25].

This paper deals with the electrodeposition of low Ru content Pt–Ru catalysts on glassy carbon and the determination of kinetic parameters of methanol electrooxidation in acid media.

2 Experimental

2.1 General aspects

Electrochemical measurements were carried out in a conventional glass cell at temperature between 23 and 50 °C. The working electrode was a glassy carbon (GC) disc of 0.07 cm^2 geometric area. The electrode surface was mechanically polished with emery paper (grit 1200) and alumina of grade 1 and 0.3 μm. The electrodeposition of Pt–Ru catalysts supported on glassy carbon (Pt–Ru/GC) were done in 0.5 M H_2SO_4 containing 2 mM H_2PtCl_6 and different concentrations of $RuCl_3$ (0, 2, 4 and 10 mM) applying a potential of −0.2 V with a total coulombic charge of 0.5 C cm^{-2}.

The counter electrode was a platinum sheet separated from the main electrolyte compartment by a porous glass diaphragm. A saturated calomel electrode (SCE) connected to the cell by a Luggin capillary served as the reference electrode (+0.241 V vs. RHE). All potentials mentioned in this work are referred to this electrode.

The kinetics of methanol oxidation between 0 and 0.6 V was determined by slow scan (1 mV s^{-1}) linear sweep voltammetry in N_2 purged H_2SO_4 solution. Methanol concentration was varied in the range 0.1–2 M CH_3OH, and H^+ concentration was modified by changing the pH between 0.4 and 2.1. All solutions were prepared with bidistilled water and analytical grade chemicals and deareated by bubbling with purified nitrogen. Current densities are referred to the real surface area, determined as described in the following section.

Conventional electrochemical techniques, linear and cyclic voltammetry and chronoamperometry, were performed with a PAR 273 potentiostat and a Voltalab PGZ-301. The morphology of the catalyst surface and the particle size were analyzed by scanning electronic microscopy (SEM, JEOL 100). Bulk compositional analysis of the Pt–Ru catalyst was performed using an X-ray detector for energy dispersive spectroscopy analysis (EDX).

2.2 Surface area determination

The active surface area of the Pt–Ru electrocatalysts was determined by underpotential deposition of copper (Cu-UPD), which was shown to be a promising method applicable for Pt–Ru electrocatalysts [26]. The working electrodes were prepared with the same method as for the electrochemical tests. First reference voltammograms were obtained in 0.1 M H_2SO_4 cycling between −0.25 to 0.8 V at a scan rate of 10 mV s^{-1}. The electrodes were polarized at 0 V for 300 s to reduce the RuO_x formed during the cyclic voltammetry.

The Cu-UPD experiments were carried out in 0.1 M H_2SO_4 and 2 mM $CuSO_4$ solution. The working electrodes were polarized at 0.059 V for 300 s to form a monolayer of copper on the catalyst surface. A linear voltammetric scan with a scan rate of 10 mV s^{-1} was then performed between 0.059 to 0.8 V to remove the adsorbed copper monolayer. The charges obtained for the copper stripping were corrected for the charges associated with background processes and oxide growth by subtracting the charge obtained from the reference scan in the same potential range. All Cu-UPD measurements were performed at room temperature.

The integration of the peak area corresponding to the Cu-UPD stripping was used to determine the electroactive surface area, with the assumption of an adsorption ratio of a single Cu atom to each surface metal atom and a monolayer charge of 420 μC cm^{-2}.

3 Results and discussion

3.1 Characterization of the catalyst

The atomic composition of Pt–Ru/GC deposits determined by EDX as a function of the concentration ratio of chloroplatinic acid to ruthenium chloride is shown in Table 1. The proportion of deposited ruthenium to platinum is lower than expected, taking into account that the molar ratio of $RuCl_3$ concentration to H_2PtCl_6 concentration is equal to one or higher. A possible explanation is that at the potential used in this work (−0.2 V vs. SCE), Pt deposition occurs at limiting current density [26] while ruthenium deposition occurs under mixed control conditions and the amount of the deposited metal is not directly proportional to

Table 1 Composition of Pt–Ru bimetallic catalysts electrodeposited on glassy carbon

$[H_2PtCl_6]/[RuCl_3]$	At.% Ru	Surface area (cm^2)	
		Cu stripping	H adsorption[a]
Pt	–	2.96	3.00
1:1	7	2.90	
1:2	14	2.86	
1:5	18	2.41	

[a] Calculated assuming that to form a monolayer of adsorbed hydrogen per cm^{-2} of smooth Pt is necessary a charge of 210 μC

concentration. Furthermore, it is possible that the existence of adsorbed hydrogen on the platinum surface blocked metal ion access to the electrode surface inhibiting metal deposition. On the other hand, it is known that in the case of a smooth ruthenium layer the ionization of hydrogen at −0.2 V is accompanied by the adsorption of water on ruthenium atoms and this process might affect the metal deposition [27–29].

Cyclic voltammograms of Pt–Ru catalysts in the absence of methanol are shown in Fig. 1. The anodic limit was set to 0.5 V to prevent anodic dissolution of ruthenium and to minimize the effect of the electrochemical treatment on the deposit structure. The disappearance of hydrogen absorption/desorption peaks with increasing ruthenium content and the high current in the double-layer region ascribed to the adsorption of oxygen-containing species on Ru atoms are characteristic of this system [11, 24, 30–32].

Some experiments were conducted by setting the anodic limit to 1.0 V to evaluate the stability of the bimetallic deposit. When ruthenium is deposited on platinum, the characteristic features of ruthenium disappear after a few sweeps. This effect is attributed to the dissolution of ruthenium [24, 33]. However, this effect was not observed with the mixed Pt–Ru electrodeposits. The voltammograms obtained after several sweeps exhibited no modifications. This behavior is associated with the formation of alloys, with ruthenium dispersed in the platinum matrix [34].

SEM micrographs of Pt–Ru deposited on glassy carbon from solutions of different composition under similar conditions are shown in Fig. 2. Electrodeposited platinum particles generally exhibit uniform size and hemispherical shape and appear regularly distributed over the support surface [9]. Ruthenium co-deposition does not modify the morphology appreciably, but a significant increase in particle size is observed. Due to the long deposition time, nearly 60 min, particles tend to coalesce and to overlap one with the other, although the existence of smaller particles suggests that new nucleus are formed throughout all the process. The SEM images show metallic agglomerates with sizes between 200 and 500 nm, and between 30 and 90 nm.

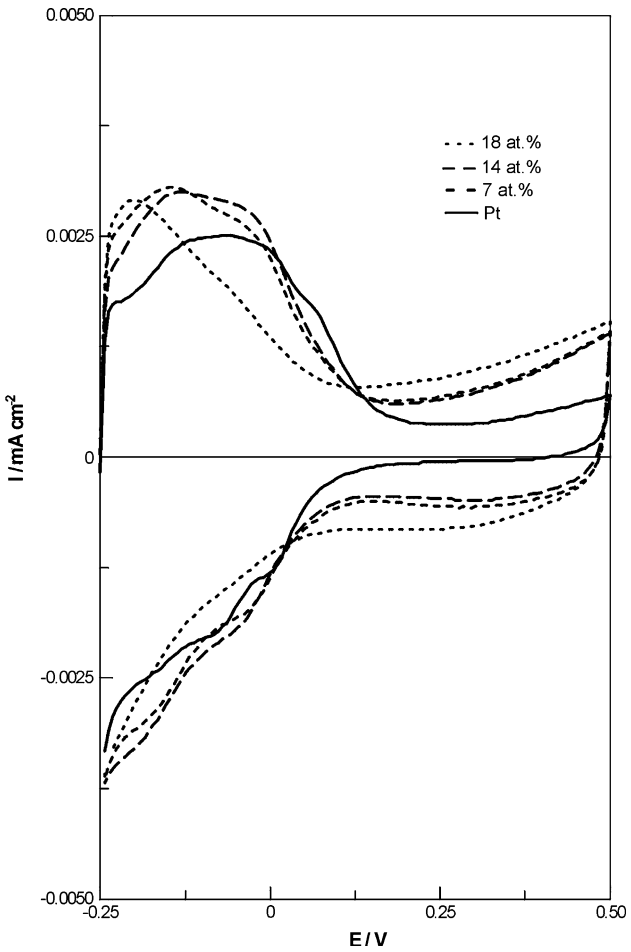

Fig. 1 Cyclic voltammograms of Pt–Ru/GC catalysts in 0.5 M H_2SO_4 at 23 °C. Sweep rate 50 mV s^{-1}

These aggregates are constituted of smaller particles. The average size of the particle measured by XRD and AFM is around 5–8 nm, in accordance with the sizes obtained by Coutanceau et al. [1] with electrodes prepared by galvanostatic pulsed electrodeposition.

Scanning electron microscopy and EDX were used to determine the spatial distribution of platinum and ruthenium. Both metals are located in the same place on the electrode surface. This result can be correlated with the data obtained from cyclic voltammetry which indicate that the metallic phase is mainly an alloy of platinum and ruthenium.

3.2 Methanol oxidation

3.2.1 Potentiodynamic measurements

Figure 3 shows the cyclic voltammetry curves recorded for the different Pt–Ru/GC electrodes at 23 °C. In the presence of methanol, it is known that the peaks of adsorbed hydrogen are depressed due to the adsorbed methanol

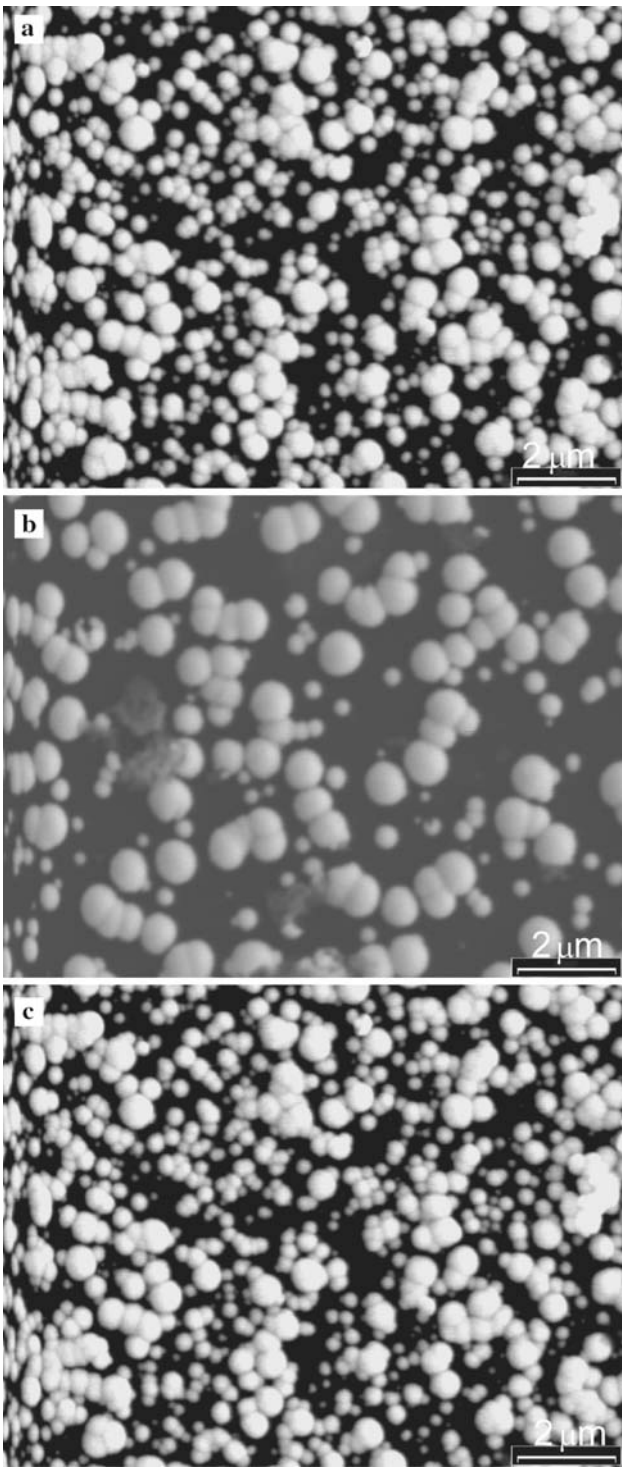

Fig. 2 Top-view SEM image of Pt–Ru/GC electrodes comparing the particles obtained using different concentrations of chloroplatinic acid and ruthenium chloride. (**a**) Platinum; (**b**) $[H_2PtCl_6]/[RuCl_3] = 1{:}1$; (**c**) $[H_2PtCl_6]/[RuCl_3] = 1{:}5$

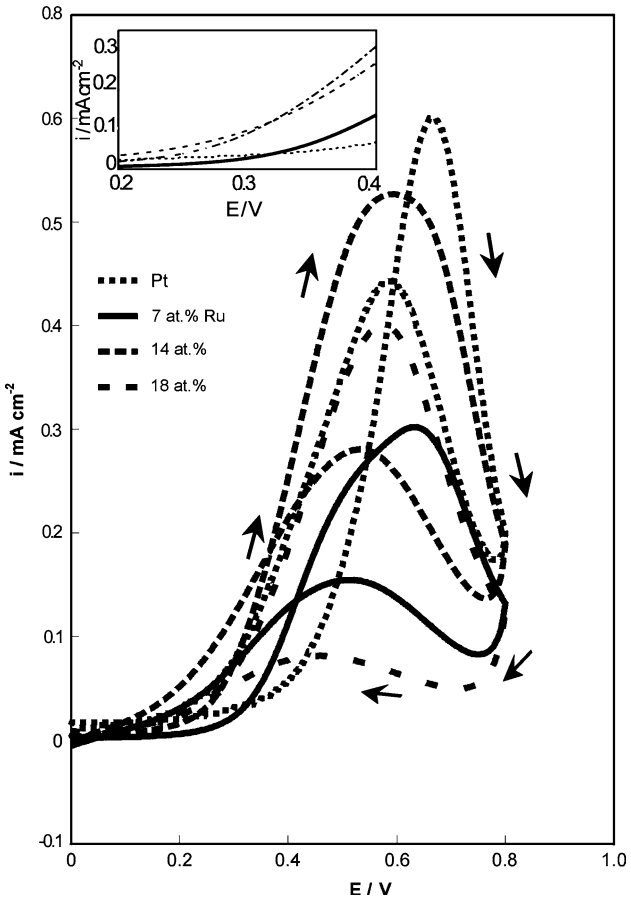

Fig. 3 Cyclic voltammograms for the oxidation of 1 M CH_3OH in 0.5 M H_2SO_4 at Pt–Ru/GC electrodes of different composition. The inset is a magnification of the potential region between 0.2 and 0.4 V. Sweep rate 50 mV s^{-1}, $T = 23$ °C

species [12, 35]. For the Pt–Ru/GC electrodes the onset of the methanol oxidation reaction takes place near 0.2 V. On the other hand, at the Pt/GC electrode the oxidation begins at 0.4 V, although the peak current density is higher. This displacement in the beginning of methanol oxidation is associated with the formation of OH_{ads} species on Ru atoms originating in the water dissociation that occur at more negative potentials (approximately 0.3 V) that on Pt atoms, through the so called bifunctional mechanism [25, 36]. The potentiodynamic curves (inset Fig. 3, Fig. 4a, b) show that between 0.2 and 0.4 V the most efficient catalyst to oxidize methanol is the alloy with 18 at.% of Ru followed by the catalyst with 14 at.% Ru. In the range 0.4–0.6 V the activities are reversed. For potentials greater than 0.6 V Pt is the best catalyst because the OH_{ads} groups are formed on atoms of Pt, whereas on atoms of Ru irreversible oxides of the type $RuO_2{\cdot}xH_2O$ ($x = 4$–5) [27], non-active for CO_{ads} oxidation are formed, reducing the active area of the catalyst.

Figure 4c shows the effect of methanol concentration on the activity of all the catalysts at 0.3 V. For all the concentrations of methanol the most effective catalyst is the alloy with 18 at.% Ru. The increase in catalyst activity from 0.1 to 1 M CH_3OH, is due to an increase of the most stable product CO on the surface [37, 38]. For 1.5 M

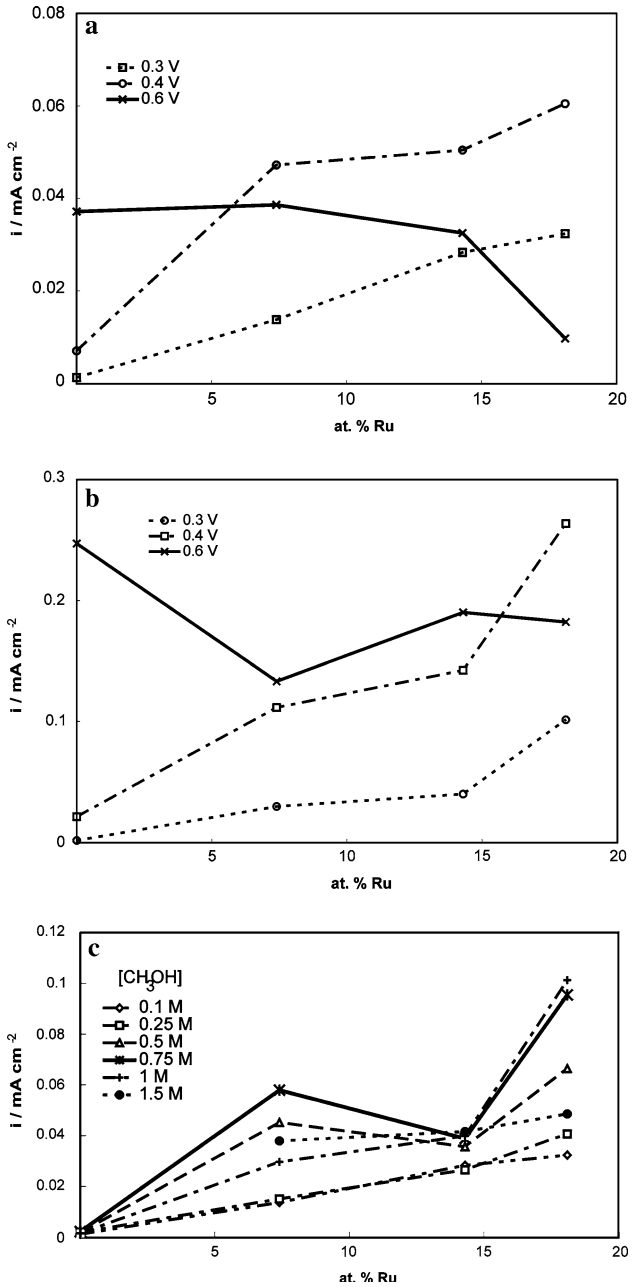

Fig. 4 Dependence of the current density with the catalyst composition at 23 °C at selected potentials in (**a**) 1 M CH_3OH + 0.5 M H_2SO_4, (**b**) 0.1 M CH_3OH + 0.5 M H_2SO_4. (**c**) Dependence of the current density with the methanol concentration at 0.3 V

CH_3OH the activity of the electrodes diminishes because the amount of formed intermediates is so high that they block active sites, inhibiting methanol oxidation.

3.2.2 *Potentiostatic measurements*

Tafel plots derived from the polarization curves for different methanol concentrations are given in Fig. 5. In the low concentration range up to 0.7 M CH_3OH, the reaction

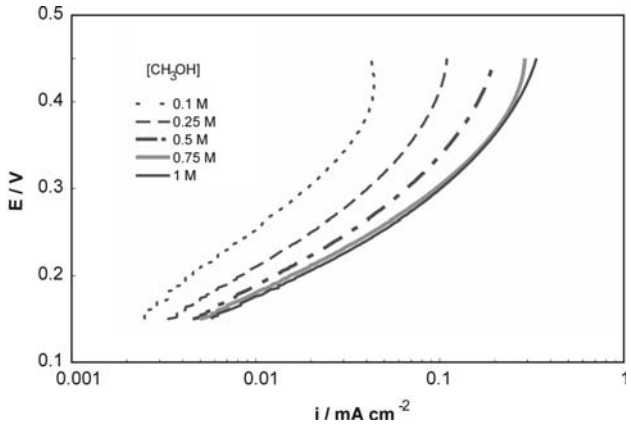

Fig. 5 Tafel plots for methanol oxidation at Pt–Ru/GC (18 at.% Ru) showing the influence of methanol concentration at $T = 23$ °C. Sweep rate 1 mV s^{-1}

rate rises with the increasing methanol concentration. For the higher concentrations, the tendency appears more erratic, and the performance of the electrodes at 1.5 M CH_3OH diminishes.

The kinetic parameters for methanol oxidation, obtained in the potential region in which the quasi steady-state curve for Pt–Ru/GC electrodes obeys a Tafel-type equation, are shown in Table 2. Although the linear region was not wide enough in all cases, between 0.15 and 0.35 V (activation-controlled region), slopes were determined with a reasonable level of accuracy, while in the higher potential region (from 0.35 to 0.5 V), limiting currents were recorded. The slope of the Tafel plots, 2.303 RT/βF, was found to depend on the ruthenium content. The lower slope was determined for the Pt catalyst, varying between 100 and 120 mV dec^{-1}. The values calculated for the alloys were higher, ranging from 120 to 140 mV dec^{-1}.

In order to determine formal reaction orders with respect to methanol, polarization curves were obtained at 23 °C in 0.5 M H_2SO_4 solutions with methanol concentration of 0.1–2 M. The methanol oxidation rate, in terms of current density, at constant potential was plotted as a function of the methanol concentration (Fig. 6). Results are summarized in

Table 2 Kinetic parameters for Pt–Ru/GC electrodes of different composition

At.% Ru	Tafel slope[a] (mV dec^{-1})	Reaction order $-CH_3OH$	Reaction order $-H^+$	$E^{b}_{a,\ app}$ (kJ mol^{-1})
0	100–120	0.5	–	58.8
7	120–130	0.7	−0.15	33.7
14	120–130	0.7	−0.3	33.6
18	130–140	0.8	−0.4	34.2

[a] At temperatures between 23 and 50 °C, in 1 M CH_3OH + 0.5 M H_2SO_4

[b] At 0.3 V, in 1 M CH_3OH + 0.5 M H_2SO_4

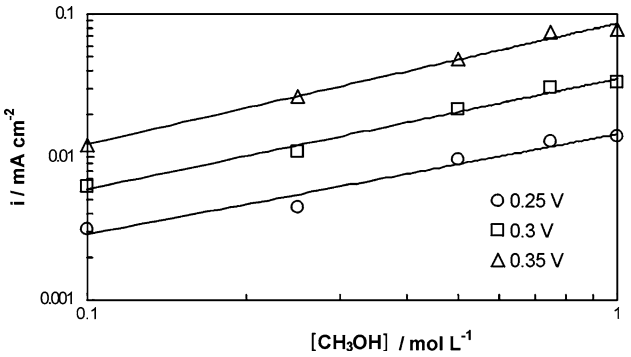

Fig. 6 Methanol oxidation currents at constant potential on Pt–Ru/GC (18 at.% Ru) as a function of concentration of methanol in 0.5 M H_2SO_4

Table 2. The reaction order for methanol varies from 0.5 to 0.8, increasing with ruthenium content increases.

The influence of the concentration of H^+ ions was also investigated in the electrolytes containing 0.1 M CH_3OH and different concentrations of H_2SO_4 at 23 °C. Reaction order is defined as the concentration dependence of log *i* at a constant potential [30]

$$\mathrm{pH} = \left(\frac{\mathrm{d}\log i}{\mathrm{d}\log[\mathrm{H}^+]}\right)_{\mathrm{E},[\mathrm{CH_3OH}]} \quad (1)$$

In the pH range 0.1 and 2, a linear dependence with negative slope was observed for the Pt–Ru/GC electrodes. The calculated reaction orders were found to change for the different alloys, varying from −0.2 to −0.4.

Polarization curves for methanol oxidation in electrolyte containing 1 M CH_3OH + 0.5 M H_2SO_4 were recorded in the temperature range 23–50 °C. The activity of the different catalysts, as measured by the current density at 0.3 V, increases with temperature. The effect is more pronounced with 18 at.% Ru alloy.

The Arrhenius plot for one of the three catalysts for the potentials within the linear Tafel region is given in Fig. 7.

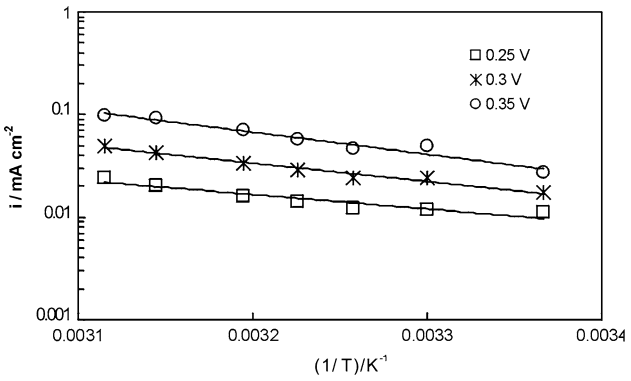

Fig. 7 Arrhenius plots for Pt–Ru/GC (18 at.% Ru) in 1 M CH_3OH + 0.5 M H_2SO_4. Data taken from the Tafel plots at the potentials indicated on the diagram

The apparent activation energy calculated from these plots vary with catalyst composition, showing lower values around 30 kJ mol^{-1} for alloys, and a higher value of 58.8 kJ mol^{-1} for platinum. Differences between activation energies of alloys of different composition have been observed by Gasteiger et al. [25], who reported values of 30 kJ mol^{-1} for an alloy of 7 at.% Ru, and 60 kJ mol^{-1} for alloys of 33 and 46 at.% Ru. Other authors have reported values of 58 kJ mol^{-1} for catalysts of 50 at.% Ru [39], 70 kJ mol^{-1} for Pt–Ru 40 mass% [24], 38 kJ mol^{-1} for electrodeposited Pt–Ru alloys [14], 20–33 kJ mol^{-1} for Pt–Ru electrodeposited on Nafion® [12], and 46.5 kJ mol^{-1} for Pt and 40.6 kJ mol^{-1} for Pt_3Ru_2 catalysts in alkaline medium [40]. High apparent activation energy values can be attributed to reaction between adsorbed CO and OH [24], or to dissociative adsorption of methanol [25], while low apparent activation energy values can be ascribed to CO surface diffusion [25], heterogeneous electrocatalytic processes [31], or mixed activation–adsorption control [15].

Nevertheless, discussion of the reaction mechanism using only the apparent activation energy is incomplete. It is necessary to take into account the apparent reaction order, Tafel slopes, surface coverage with adsorbed species, particle size, etc.

According to Léger [41] for the elucidation of the reacting mechanism, knowledge of the following items are vital: (i) identification of the reaction products and determination of the electrode kinetics of the different reactions, (ii) identification of all the adsorbed intermediate species and their distribution on the electrode surface, and (iii) identification of the electrode kinetics of the intermediate steps in the overall mechanism and correlation with the structure and composition of the electrocatalyst surface. The effect of ruthenium in bimetallic Pt–Ru systems is explained by a bifunctional reaction mechanism [30, 36] such as shown below. In the temperature range between 23 and 50 °C, CH_3OH is adsorbed only on Pt sites. The interaction between CH_3OH and Ru is a strongly activated process correlated with a high energy of adsorption of oxygen on Ru (≈330 kJ mol^{-1} for atomic oxygen) [25]. Water dissociates on Ru giving OH_{ads} (step 4) and the species adsorbed on Pt and Ru combine together forming CO_2 (step 5) in a Langmuir–Hinshelwood (L–H) type reaction [30].

$$\mathrm{CH_3OH + Pt \rightarrow Pt\text{-}CH_3OH_{ads}} \quad (2)$$

$$\mathrm{Pt\text{-}CH_3OH_{ads} \rightarrow Pt\text{-}CO_{ads} + 4H^+ + 4e^-} \quad (3)$$

$$\mathrm{H_2O + Ru \rightarrow Ru\text{-}OH_{ads} + H^+ + e^-} \quad (4)$$

$$\mathrm{H_2O + Pt \rightarrow Pt\text{-}OH_{ads} + H^+ + e^-} \quad (4')$$

$$\mathrm{Pt\text{-}CO_{ads} + Ru\text{-}OH_{ads} \rightarrow Pt + Ru + CO_2 + H^+ + e^-} \quad (5)$$

$$\mathrm{Pt\text{-}CO_{ads} + Pt\text{-}OH_{ads} \rightarrow 2Pt + CO_2 + H^+ + e^-} \quad (5')$$

For the Pt/GC electrode an apparent activation energy of 58.8 kJ mol^{-1}, Tafel slopes in the range of 100–120 mV dec^{-1}, and half order kinetics with respect to methanol (see Table 2), were determined. These values are reasonable if the step 5′ (L–H reaction) is the rate determining step (rds). The half order kinetics with respect to methanol concentration (0.1–1 M) is in accordance with that determined by other authors [12, 36, 42–44], indicating Temkin adsorption. In the same way the Tafel slopes between 100 and 120 mV dec^{-1} are similar to that found by Bagotzky et al. [36]. The variation in the values in the range 100–120 mV dec^{-1} may be explained considering that at high potentials the adsorbed CO itself becomes more susceptible to nucleophilic attack giving a lower Tafel slope [45]. Finally the apparent activation energy is bigger than that obtained for other authors. For example values as low as 20–33 kJ mol^{-1} on Pt/SPEs [12] have been reported, and 35 kJ mol^{-1} on Pt/Nafion® 117 [46], and 39.8 kJ mol^{-1} on smooth Pt [36] but 53 kJ mol^{-1} to activation energy for CO_{ads} surface diffusion on Pt(111) [47].

It is clear that CO_{ads} diffusion toward Pt–OH_{ads} sites is involved in the rate determining step. Diffusion may be complicated by the presence of other methanolic species adsorbed on the catalyst surface [24], and by the specific adsorption of bisulfate anions [32, 48].

Finally the difference between the apparent activation energy determined in this work and that found in the literature might be due to the morphology, size and distribution of particles on the substrate or to the deposits roughness. On the other hand, lower values of apparent activation energy were determined for Pt–Ru/GC electrodes, and the Tafel slopes were between 120 and 140 mV dec^{-1} (see Table 2).

The reaction order with respect to methanol concentration (0.1–1 M) between 0.7 and 0.8 was determined; while reaction orders with respect to solution pH between −0.15 and −0.4 for the different alloys were found.

Apparent activated energies determined in ours experiences were similar to those determined by Gasteiger et al. [25] for PtRu alloys with 7 at.% Ru (30 kJ mol^{-1}). Considering this coincidence, we expected step 5 (L–H reaction), to be the rate determining step. The lower apparent activated energies determined on Pt–Ru/GC alloys in comparison with that determined on Pt/GC might be explained of the facile generation of OH_{ads} on Ru atoms at 0.3 V, since the CO_{ads} molecules can migrate from Pt sites to Ru sites where OH_{ads} nucleation occurs. The Tafel slope values agree with those determined by other author [12, 24, 36] that considered the step 5 as the rds.

The negative reaction orders with respect to pH suggest that OH_{ads} species are involved in the rate determining step [24, 43].

The reaction order with respect to CH_3OH concentration are slightly higher than 0.5 (formal reaction order) [24, 31, 36, 43], but these order are similar to that determined by Vidaković et al. [39] at 0.5 V vs. SHE.

It was determined experimentally that CO_{ads} is the most stable product formed during methanol oxidation [37, 38], but other adsorbed species such as CH_3O, –CHOH, and –COOH have also been identified by RMN, DEMS, ECTDMS, and SNIFTIRS [49–54]. These are less stable intermediaries that difficult CO diffusion towards OH_{ads} sites. The presence of Ru in the electrodes, forming an alloy with Pt permits the formation of OH_{ads} groups at lower potentials than on Pt/GC electrodes, favoring oxidation of adsorbed CO, which must migrate smaller distances to oxidize to CO_2.

4 Conclusions

Methanol oxidation in acid media was studied on Pt–Ru electrocatalysts with low ruthenium content supported on glassy carbon. Cyclic voltammetry of the electrocatalyst reflects the amount of ruthenium in the sample, through the modification observed in the processes associated to hydrogen adsorption.

Kinetic parameters were determined for methanol electrooxidation. The slope of the Tafel plots was found to depend on the ruthenium composition. The lower slope was determined for the Pt catalyst, varying between 100 and 120 mV dec^{-1}. The values calculated for the alloys were higher, ranging from 120 to 140 mV dec^{-1}. The reaction order for methanol varies from 0.5 to 0.8, increasing when the ruthenium content augments.

The activation energy calculated from Arrhenius plots was found to change with the catalyst composition, showing the lower value of 30 kJ mol^{-1} for the alloys, and the higher value, of 58.8 kJ mol^{-1}, for platinum.

The effect of ruthenium in bimetallic Pt–Ru systems is explained by bifunctional reaction mechanism. In all the electrodes studied, surface diffusion of CO_{ads} is the rate limiting step in the reaction through Langmuir–Hinshelwood (L–H) type reaction. The morphology and size of the agglomerates have some influence in the methanol reaction.

Kinetics of methanol oxidation taking place on the different electrodes have been analyzed considering: (i) the nature of the stable adsorbed species resulting from methanol adsorption and dehydrogenation, (ii) the effect of Ru atoms, and (iii) morphology and size of the agglomerates.

Acknowledgements This work was supported by ANPCYT grant No 10-11133, UNS grant 24/M097 and CIC. J.M.S. is grateful to the CONICET for a doctoral fellowship.

References

1. Coutanceau C, Rakotondrainibe AF, Lima A, Garnier E, Pronier S, Léger J-M, Lamy C (2004) J Appl Electrochem 34:61
2. Wilson MS, Gottesfeld S (1992) J Appl Electrochem 22:1
3. Gottesfeld S, Zawodzinski TA (1997) In: Alkire RC, Gerischer H, Kolb DM, Tobias CW (eds) Advances in electrochemical science and engineering, vol 5. Wiley-VCH, Weinheim, Germany, p 125
4. Sasikumar G, Ihm JW, Ryu H (2004) Electrochim Acta 50:601
5. Wei ZD, Chan SH (2004) J Electroanal Chem 569:23
6. Rao CRK, Trivedi DC (2005) Coord Chem Rev 249:613
7. Wei ZD, Chan SH, Li LL, Cai HF, Xia ZT, Sun CX (2005) Electrochim Acta 50:2279
8. Shen M, Roy S, Scott K (2005) J Appl Electrochem 35:1103
9. Hogarth MP, Punk J, Shukla AK, Hamnett A (1994) J Appl Electrochem 24:85
10. Duarte MME, Pilla AS, Sieben JM, Mayer CE (2006) Electrochem Comm 8:159
11. Maillard F, Gloaguen F, Léger J-M (2003) J Appl Electrochem 33:1
12. Aramata A, Kodera T, Masuda M (1988) J Appl Electrochem 18:577
13. Niu L, Li Q, Wei F, Wu S, Liu P, Cao X (2005) J Electroanal Chem 578:331
14. Lee C-H, Lee C-W, Kim D-I, Bae S-E (2002) Int J Hydrogen Energy 27:445
15. Tusseeva EK, Mikhaylova AA, Khazova OA, Kourtakis K-D (2004) Russian J Electrochem 40:1146
16. Chrzanowski W, Wieckowski A (1997) Langmuir 13:5974
17. Vigier F, Gloaguen F, Léger J-M, Lamy C (2001) Electrochim Acta 46:4331
18. Iúdice de Souza JP, Iwasita T, Narta EC, Vielstich W (2000) J Appl Electrochim 30:43
19. Rodríguez-Nieto FJ, Morante-Catacora TY, Cabrera CR (2004) J Electroanal Chem 571:15
20. Selvaraju T, Ramaraj R (2005) J Electroanal Chem 585:290
21. Ross PN Jr (1998) In: Lipkowski J, Ross PN (eds) Electrocatalysis. Wiley-VCH, New York, p 43
22. Wasmus S, Küver A (1999) J Electroanal Chem 461:14
23. Liu H, Song C, Zhang L, Zhang J, Wang H, Wilkinson DP (2006) J Power Sources 155:95
24. Gojković SL, Vidaković TR, Durović DR (2003) Electrochim Acta 48:3607
25. Gasteiger HA, Markovic N, Ross PN, Cairns E (1994) J Electrochem Soc 141:1795
26. Green CL, Kucernak A (2002) J Phys Chem B 106:1036
27. Vuković M, Čukman D (1999) J Electroanal Chem 474:167
28. Hadži-Jordanov S, Argerstein H, Vuković M, Conway BE (1977) J Phys Chem 81:2271
29. Hepel T, Pollak FH, O'Grady WE (1984) J Electrochem Soc 131:2094
30. Watanabe M, Motoo S (1975) J Electroanal Chem 60:267
31. Chu D, Gilman S (1996) J Electrochem Soc 143:1685
32. Tripković AV, Popović KD, Grgur BN, Blizanac B, Ross PN, Marković NM (2002) Electrochim Acta 47:3707
33. He C, Kunz HR, Fenton JM (1997) J Electrochem Soc 144:970
34. Rauhe BR, McLarnon FR, Cairns E (1995) J Electrochem Soc 142:1073
35. Wang K, Gasteiger HA, Markovic NM, Ross PN Jr (1996) Electrochim Acta 41:2587
36. Bagotzky VS, Vassilyev YB (1967) Electrochim Acta 12:1323
37. Seiler T, Savinova ER, Friedrich KA, Stimming U (2004) Electrochim Acta 49:3927
38. Jusys Z, Behm RJ (2001) J Phys Chem B 105:10874
39. Vidaković T, Christov M, Sundmacher K (2005) J Electroanal Chem 580:105
40. Tripković AV, Štrbac S, Popović KD (2003) Electrochim Comm 5:484
41. Léger J-M (2001) J Appl Electrochem 31:767
42. Gojković SL, Vidaković TR (2001) Electrochim Acta 47:633
43. Gojković SL (2004) J Electroanal Chem 573:271
44. Tripković AV, Popović KD, Lović JD, Jovanović VM, Kowal A (2004) J Electroanal Chem 572:119
45. Christensen PA, Hammett A, Trougton GL (1993) J Electroanal Chem 362:207
46. Méli G, Léger J-M, Lamy C, Durand R (1993) J Appl Electrochem 23:197
47. Kwasniewski VJ, Schmidt DL (1992) Surf Sci 274:329
48. Davies JC, Hayden BE, Pegg DJ, Rendall ME (2002) Surf Sci 496:110
49. Arico A, Srinivasan S, Antonucci V (2001) Fuel Cells 1:133
50. Khazova O, Mikhailova A, Skundin A, Tuseeva E, Havranek A, Wippermann K (2002) Fuel Cells 2:99
51. Jusys Z, Behm RJ (2001) J Phys Chem B 105:10874
52. Iwasita T, Vielstich W, Santos E (1987) J Electroanal Chem 229:367
53. Willsau J, Wolter O, Heitbaum J (1985) J Electroanal Chem 185:163
54. Jarvi TD, Stuve E M (1998) In: Lipkowski J, Ross PN (eds) Electrocatalysis. Wiley-VCH, USA, p 75